ECS Transactions, 78 (1) 1245-1252 (2017)
10.1149/07801.1245ecst ©The Electrochemical Society

Synthesis of Ru-doped Double Perovskite Anode for SOFC

N. K. Monteiro, G. A. S. Candido and F. C. Fonseca

Institute of Energy and Nuclear Research, University of São Paulo, São Paulo, Brazil

$Pr_{0.5}Ba_{0.5}MnO_3$ was studied as the precursor phase of the double perovskite $PrBaMn_2O_{5+\delta}$ (PBMO) anode material for solid oxide fuel cells (SOFC). The general properties were studied in both the pristine compound and Ru-doped samples $Pr_{0.5}Ba_{0.5}Mn_{1-x}Ru_xO_3$ (PBMRu). Ru substitution at the B-site is expected to enhance the catalytic properties of the ceramic towards ethanol or methane fuels. The studied compounds were synthesized by the polymeric precursor method and characterized by thermogravimetric analyses, X-rays diffraction (XRD), and electrical transport properties. The experimental data show PBMO phase formation occurring at ~800°C and single phase compounds at ~1100°C up to ~10 at.% of Ru substituted. Similar ionic radius of Ru^{3+} and Mn^{3+} results in little effect on both the crystalline structure and electrical conductivity as compared to the pristine compound.

Introduction

Despite the great efforts in recent years to develop alternative ceramic anodes, such oxides do not exhibit performance to match those of the standard Ni cermet (1). Ceramic anodes have their applications in solid oxide fuel cell (SOFC) limited by their low chemical stability, low compatibility with other components and/or low durability. Thus, there are scarce single-phase compounds capable to meet the requirements of an SOFC electrode (2). Nonetheless, several candidates have been reported such as titanates ($ATiO_3$, where A = Ca, Sr, Ba, La), $La_{1-x}Sr_xCrO_3$, with partial atomic substitutions of Cr by several metals such as Ru, Ni, Pd, Mn, Fe and Co (1,3-6). In this family $La_{1-x}Sr_xCrO_3$, stands out the $La_{0.75}Sr_{0.25}Cr_{0.5}Mn_{0.5}O_{3-\delta}$ compound, which showed good performance at high temperatures for direct oxidation of hydrocarbons (7-9).

Ceramic oxides with perovskite type crystalline structure usually have improved performance as SOFC anodes when doped with transition metals (10-16). Several studies have verified that these compounds may exhibit important properties, such as mixed ionic-electronic conductivity, controlled by doping. In comparison to the simple perovskite ABO_3, the double perovskite structure $AA'BB'O_6$, has also gained interest due to its extraordinary electrochemical performance, high redox stability and convenient thermal expansion coefficient. This family of compounds can be understood as repeated sequences of $|AO||BO_2||A'O||B'O_2|$ that provides a great potential to weaken the oxygen binding force and create a high amount of oxygen vacancies, with high mobility (1,15,17,18).

In this context, some reports have shown ceramic anodes doped with metals, such as Ni, Ru, Pt, Mo, or ceramic phases (mostly ceria-based), aiming at improved catalytic

properties for use with different fuels in SOFCs (1,6,19-21). Impregnation, in which a suspended metal salt (7) is deposited on the electrode is a common method used for adding a second phase to the ceramic anode. However, this method can lead to nanoparticles inhomogeneous distribution and nanoparticles highly susceptible to coarsening at high temperature (14,18,22,23). An alternative method is the incorporation of the metal cation in the crystalline structure of the ceramic compound followed by exsolution of metallic particles promoted by a thermal treatment in reducing conditions (7,13,14,22-24). Such nanoparticles precipitate with rather uniform dispersion on the surface of the matrix compound and exhibit a strong interaction with the support compound that prevents coalescence (7,14,18).

Previous reports indicated that double perovskites at high temperatures and reducing atmospheres may undergo a phase transition of the crystalline symmetry, inducing the formation of a layered structure and the creation of orderly oxygen vacancies (13,14,18,22,25,26). Such transition can favor the exsolution of the dopants (14,18). Thus, the present study aims at developing ceramic with double perovskite structure to be used as anode in direct ethanol SOFC. The synthesis and characterization of the ceramic of $Pr_{0.5}Ba_{0.5}MnO_3$ (PBMO) with partial substitutions of Mn by Ru ($Pr_{0.5}Ba_{0.5}Mn_{1-x}Ru_xO_3$, PBMRu) are presented.

Experimental

$Pr_{0.5}Ba_{0.5}Mn_{1-x}Ru_xO_3$ compounds with partial substitution of ruthenium x = 0, 5, 10 and 20 at.% (PBMRux%) were prepared by the polymeric precursor technique. The synthesis of the ceramic followed the procedure detailed in Figure 1. First, the calculated amounts of the starting materials (all Sigma-Aldrich, >99%) are carefully weighted. The amounts of citric acid (CA, Fluka) and the volume of ethylene glycol (EG, Riedel-de-Häen) follow the ratio of 60:40 (CA: EG) in mass, and the molar ratio of CA to metal cations was 3:1 (27).

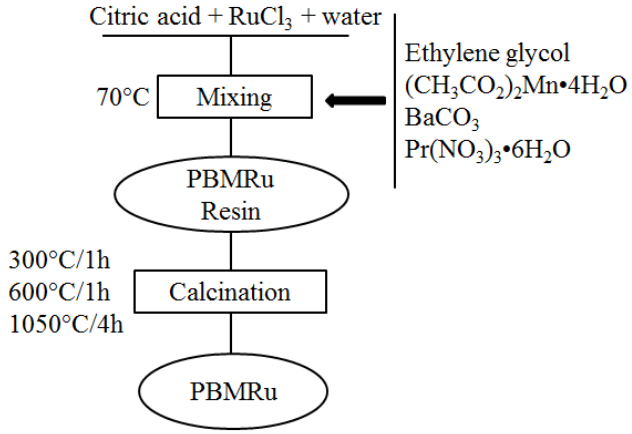

Figure 1. Diagram of the experimental procedure for the synthesis of $Pr_{0.5}Ba_{0.5}Mn_{1-x}Ru_xO_3$.

Initially, a mixture with CA, ruthenium chloride and distilled water was heated at ~70°C under constant stirring. After 15 min, ensuring complete dissolution of the salts, manganese acetate with small amount of distilled water was added to the solution under constant stirring. The remaining metallic salts were added consecutively: barium

carbonate (or barium acetate), praseodymium nitrate and EG for polymerization of the solution. The mixture was evaporated to a viscous resin that was pre-calcined at 300°C for 1 hour. Then, a pre-calcining step at 600°C for 1 hour and calcination at 1050°C for 4 hours in air were carried out for organics removal and phase formation, respectively. Cylindrical pellets were pressed (10 mm diameter) and sintered (1500 °C for 12 h). For some analyzes, calcined powders were heat treated at 1400°C for 2 h. The thermal treatment for reducing samples was performed in a tube furnace according to the following procedure: (a) heating at 10°C min^{-1} in N_2 flow (~50 $ml.min^{-1}$); (b) 800°C for 8 h in flowing 4% H_2 / 96% Ar (50 $ml.min^{-1}$) gas mixture.

The thermal decomposition of the precursor polymer resin was studied by simultaneous thermogravimetry and differential thermal analysis (TG-DTA), Labsys-Setaram, up to 1400°C with a heating rate of 10 °C min^{-1}, under synthetic air flow. Phase characterization was carried out by powder X-rays diffraction (XRD), in the 20° to 90° 2θ range, with a step of 0.05° and counting time of 2 s, using Cu Kα radiation on a Rigaku MiniFlex diffractometer. Powder morphology was analyzed by scanning electron microscopy (SEM) in a JEOL JSM-6010LA. The electric transport was studied by 4-probe method using a Lakeshore 370 ac resistance bridge. Bar samples were cut from sintered pellets and electrical contacts painted with silver ink cured at 600°C for 1 h. Measurements were performed between room temperature and 850°C, with 3 °C min^{-1} heating/cooling rate, under static air or flowing 4% H_2 / 96% Ar.

Results and Discussion

The thermal behavior of the PBMO resins was investigated by TG/DTA analysis, as shown in Figure 2.

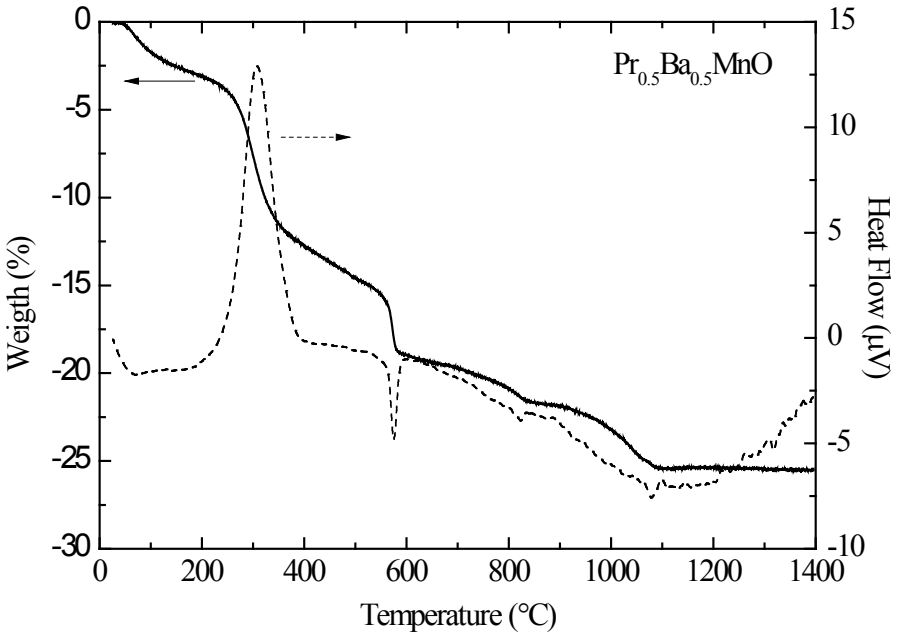

Figure 2. TG/DTA curve of the precursor resin of $Pr_{0.5}Ba_{0.5}MnO_3$.

The total mass loss up to 1400°C (~25%) occurred in three main steps: (i) loss at ~70°C, probably related to water evaporation; (ii) the most intense loss (~15%) in two steps between ~250-600°C, in which most of organic matter and volatiles are oxidized;

and (iii) between 600-1080°C due to the elimination of remaining organic matter and barium carbonate decomposition.

The prepared resins were thermally treated at different temperatures between 600°C and 1150°C to monitor phase formation. Phase formation was evaluated by XRD analysis. The Figure 3 show the evolution of XRD data of the PBMO heated at different temperatures between 600°C and 1150°C.

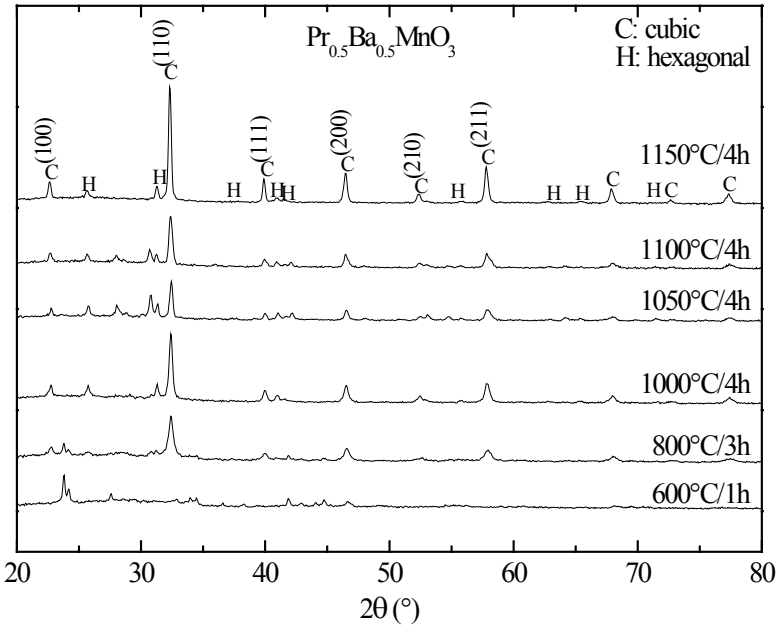

Figure 3. XRD of pre-calcined powders of PBMO (600°C or 800°C) after thermal treatment at 1000°C, 1050°C, 1100°C and 1150°C for 4 hours.

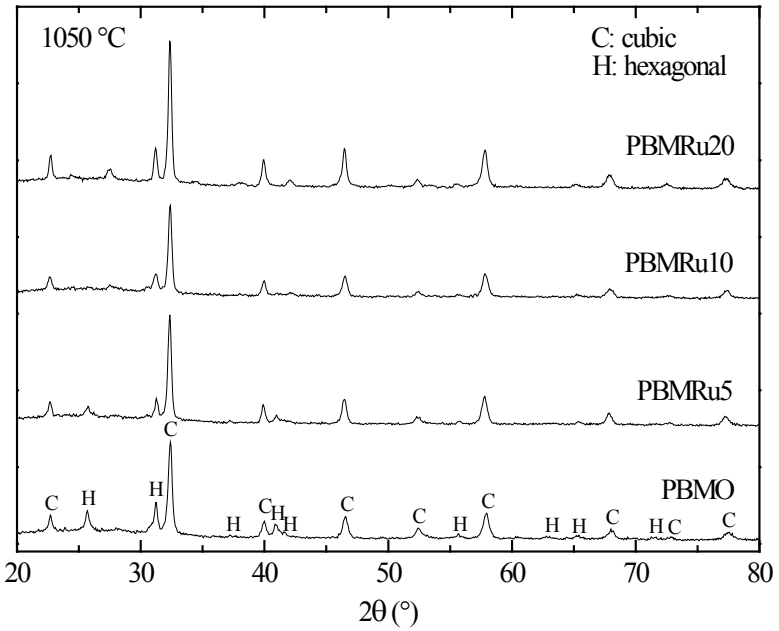

Figure 4. XRD of $Pr_{0.5}Ba_{0.5}Mn_{1-x}Ru_xO_3$ compounds calcined at 1050°C.

Second phase peaks were observed in 2θ range between 25° and 30°, possibly related to the presence of barium carbonate. Based on the preliminary results for the parent

compound, precursor resins of PBMRu were calcined at 1050 °C for 4 hours. Figure 4 shows the X-ray diffractograms of PBMRux% series (x = 0, 0.05, 0.10, and 0.20).

In Figure 4, the diffraction peaks of PBMO are observed for all compounds, suggesting the partial substitution of Mn by Ru. However, for PBMRu20 additional peaks were detected indicating a limit for Ru substitution in the PBMO structure.

The calculated lattice parameters of PBMRux are listed in Table I (28). The ionic radius of Ru^{3+} (0.680 Å) is close to that of Mn^{3+} (0.645 Å), indicating that substitution of Mn occurs with small lattice distortion (28,29).

TABLE 1. Calculated lattice parameters of the PBMRux compounds.

Compound	PBMO (28)	PBMO	PBMRu5	PBMRu10	PBMRu20
a (Å)	3.893	3.896	3.945	3.848	3.870

The PBMO compound was thermally treated in reducing atmosphere for transformation of the crystalline structure into a layered double perovskite (13,18). Figure 5 shows the XRD of the layered double perovskite PBMO (14,18).

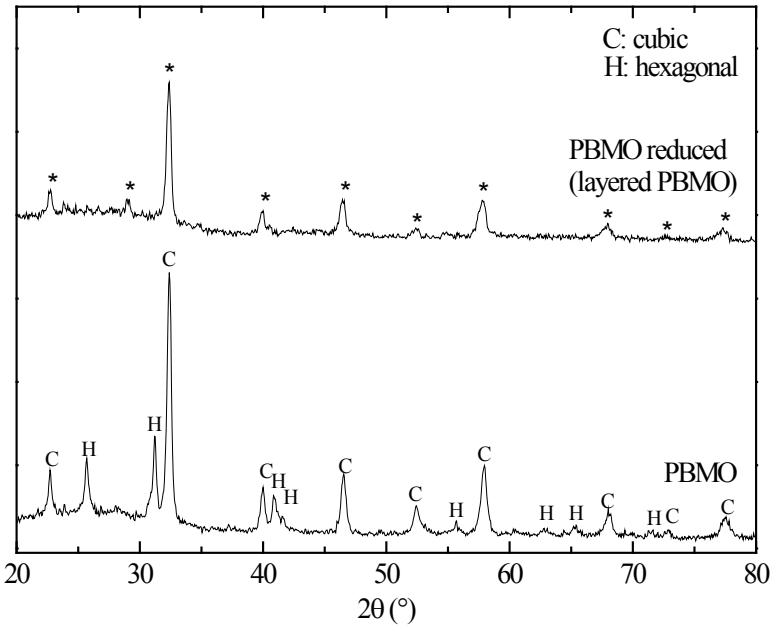

Figure 5. XRD of the phase samples PBMO and reduced layered PBMO.

Upon reducing thermal treatment, the hexagonal structure of PBMO is suppressed and the layered double perovskite exhibits cubic symmetry (13).

Figure 6 shows the temperature dependence of the electrical conductivity of PBMO under air and 4% H_2 / 96% Ar flow. PBMO is a mixed conductor (ionic and electronic), the electronic conduction results from the formation of Mn^{4+} (electronic exchange) and the ionic conduction due to the mobility of the oxygen vacancies created in the crystal lattice to ensure the electrical neutrality during the reduction process (13). Temperature dependence of the electrical conductivity follows Arrhenius behavior in both air and reducing conditions. When heating samples in reducing conditions an abrupt decrease of the electrical conductivity takes place at ~800°C, related to the reduction of the structure.

During cooling in reducing atmosphere (red) the samples follows a thermally activated behavior with higher activation energy (E_a) than in air, $E_{a,red}$ = 0.392 eV e $E_{a,air}$ = 0.101 eV.

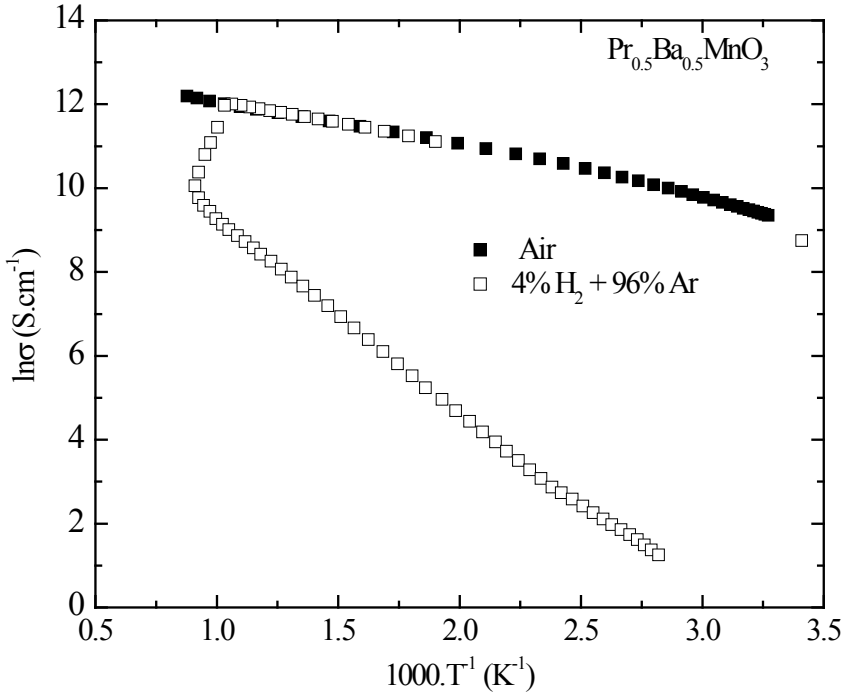

Figure 6. Temperature dependence of the electrical conductivity for PBMO under air and hydrogen.

Figure 7 shows the temperature dependence of the electrical conductivity of PBMRu10 and PBMRu20 compounds previously reduced and layered PBMO measured in flowing 4% H_2 / 96% Ar.

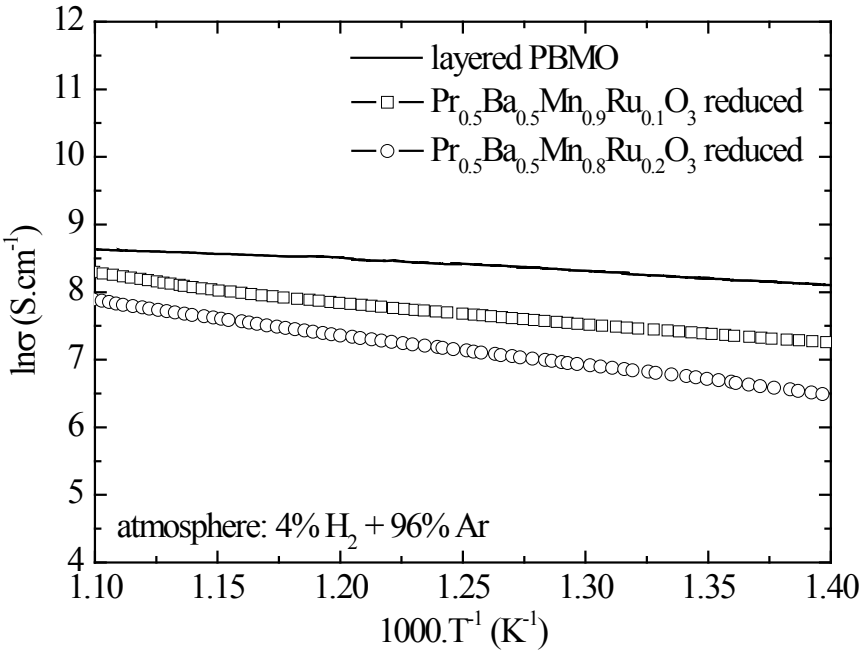

Figure 7. Temperature dependence of the electrical conductivity of $Pr_{0.5}Ba_{0.5}Mn_{1-x}Ru_xO_3$ (x = 0.10 and 0.20) previously reduced and $Pr_{0.5}Ba_{0.5}MnO_3$ in hydrogen.

It is observed that with the doping of Ru, compounds are obtained with slightly lower electrical conductivity values when compared to the PBMO value. Despite the doping of different fractions of Ru, due to the reducing atmosphere, the compounds presented light decrease in the electrical conductivity values.

Conclusion

$Pr_{0.5}Ba_{0.5}MnO_3$ (PBMO) compounds were synthesized with partial substitution of Mn by Ru. Thermal treatment at 1050°C results in single phase for the parent compound, whereas Ru-substituted samples exhibit a limit for singe phase at x ~ 0.10 at.%. Doping with Ru at B site did not alter significantly both the lattice parameters PBMO and electrical conductivity.

Acknowledgments

This work was funded by CNPq, CAPES, CNEN and FAPESP. The authors thank CNPq and CAPES for scholarships.

References

1. I. Z. Rahman, M. A. Raza and M. A. Rahman, *Advanced Materials Research*, **445**, 497 (2012).
2. J. Macek, B. Novosel and M. Marinsek, *Journal of the European Ceramic Society*, **27**, 487 (2007).
3. S. P. S. Shaikh, A. Muchtar and M. R. Somalu, *Renewable and Sustainable Energy Reviews*, **51**, 1 (2015).
4. S. Vasala and M. Karppinen, *Progress in Solid State Chemistry*, **43**, 1 (2015).
5. G. Chen, Y. M. Qian, M. Liu, W. Q. Ma, S. J. Geng, X. Y. Meng, K. Yu and G. Q. Liu, *Journal of Power Sources*, **328**, 212 (2016).
6. V. Y. Zenou, D. E. Fowler, R. Gautier, S. A. Barnett, K. R. Poeppelmeier and L. D. Marks, *Solid State Ionics*, **296**, 90 (2016).
7. L. Thommy, O. Joubert, J. Hamon and M.T. Caldes, *International Journal of Hydrogen Energy*, **41**, 14207 (2016).
8. S. Tao and J. T. S. Irvine, *Nature Materials Letters*, 2, 320 (2003).
9. F. C. Fonseca, E. N. S. Muccillo, R. Muccillo and D. Z. de Florio, *Journal of the Electrochemical Society*, **155**(5), B483 (2008).
10. C. Moure and O. Peña, *Progress in Solid State Chemistry*, **43**, 123 (2015).
11. A. Atkinson, S. Barnett, R. J. Gorte, J. T. Irvine, A. J. Mcevoy, M. Mogensen, S. C. Singhal and J. Vohs, *Nature Materials*, **3**, 17 (2004).
12. S. P. Jiang and S. H. Chan, *Journal of Materials Science*, **39**, 4405 (2004).
13. S. Sengodan, S. Choi, A. Jun, T. H. Shin, Y.W. Ju, H.Y. Jeong, J. Shin, J. T. S. Irvine and G. Kim, *Nature Materials*, **14**, 205 (2015).
14. D. Neagu, G. Tsekouras, D. N. Miller, H. Ménard and J. T. S. Irvine, *Nature Chemistry*, **5**, 916 (2013).
15. Y.H. Huang, R. I. Dass, Z.L. Xiang and J. B. Goodenough, *Science*, **312**, 254 (2006).

16. A. Chroneos, R. V. Vovk, I. L. Goulatis and L. I. Goulatis, *Journal of Alloy and Compounds*, **494**, 190 (2010).
17. Y.F. Sun, Y.Q. Zhang, J. Chen, J.H. Li, Y.T. Zhu, Y.M. Zeng, B. S. Amirkhiz, J. Li, B. Hua and J.L. Luo, *Nano Letters*, **16**(8), 5303 (2016).
18. D. K. Mahato, M. Rudra and T. P. Sinha, *Journal of Alloy and Compounds*, **689**, 617 (2016).
19. T. Takeguchi, R. Kikuchi, T. Yano, K. Eguchi and K. Murata, *Catalysis Today*, **84**, 217 (2003).
20. A. Babaei, L. Zhang, S. L. Tan and S. P. Jiang, *Solid State Ionics*, **181**, 1221 (2010).
21. Y. Gao, D. Chen, M. Saccoccio, Z. Lu and F. Ciucci, *Nano Energy*, **27**, 499 (2016).
22. C. Arrivé, T. Delahaye, O. Joubert and G. Gauthier, *Journal of Power Sources*, **223**, 341 (2013).
23. B. D. Madsen, W. Kobsiriphat, Y. Wang, L. D. Marks and S. A. Barnett, *Journal of Power Sources*, **166**, 64 (2007).
24. R. Thalinger, M. Gocyla, M. Heggen, R. D.Borkowski, M. Grünbacher, M. S. Pollach, D. Schmidmair, B. Klötzer and S. Penner, *Journal of Catalysis*, **337**, 26 (2016).
25. H. Ding, Z. Tao, S. Liu and J. Zhang, *Scientific Reports*, **5**, 18129 (2015).
26. P. A. Lessing, *Ceramic Bulletin*, **68**(5), 1002 (1989).
27. J. Clark, Calculations in AS/A Level Chemistry, Longman, Pearson Education, 2000.
28. D. C. Ling, P. C. Hsu and C. L. Lee, *Journal of Physics: Conference Series*, **400**, 032047 (2012).
29. R. Grimes, Atomic Simulation Group Database, Department of Materials, Imperial College London (link http://abulafia.mt.ic.ac.uk/shannon/ptable.php).